Accurate Modeling of Near-Wellbore Effects Induced by Supercritical CO2 Injection

Wapperom, M.B.; Lyu, X.; Voskov, D.V.

Accurate modeling of near-wellbore effects induced by supercritical CO2 injection

M. Wapperom[1], X. Lyu[1,2], D. Voskov[1,3]

[1] Delft University of Technology; [2] China University of Petroleum (Beijing); [3] Stanford University

Summary

During injection of supercritical CO2 into saline aquifers or depleted gas reservoirs, the complex interaction of CO2 and impurities with reservoir fluids plays a very important role and can significantly alternate the injectivity. Brine evaporation into the CO2-rich phase can lead to salt precipitation which will reduce the effective permeability of the porous rock. A tangible cooling of the near-wellbore region due to the Joule-Thomson effect can lead to hydrate formation which will reduce injectivity even more. Complex phase behavior of supercritical CO2 with brine and hydrocarbon components in highly heterogeneous porous media accompanied by all these phenomena will strongly affect pressure distribution which is in turn related to mechanical risks.

In this work, we present a unified simulation framework for modelling near-wellbore effects induced by supercritical CO2 injection developed in the Delft Advanced Research Terra Simulator (DARTS) platform. This framework uses the Operator-Based Linearization (OBL) technique for incorporating all complex physical phenomena in a fully coupled fully implicit manner. A general multicomponent multiphase flash based on a combination of classic cubic equations of state (e.g., Peng-Robinson) for hydrocarbon/CO2-rich phases and an activity model for the aqueous phase is implemented. Hydrate phase behavior is modelled using a modified Van der Waals-Platteeuw hydrate equation of state. Formation dry-out and salt precipitation are incorporated by using the Element Balance approach coupled with thermodynamics. Thermophysical property correlations relevant to the thermodynamic conditions of interest are implemented and validated against lab experiments.

We demonstrate that all important physical phenomena, such as the Joule-Thomson effect, hydrate formation and salt precipitation can be effectively captured by the OBL approach. We use several existing numerical benchmarks to validate the accuracy of the developed framework in the dynamic representation of all these effects. The interplay between these complex phenomena and reservoir heterogeneity is demonstrated in an unstructured heterogeneous near-wellbore reservoir model.

Introduction

During injection of supercritical CO_2 into saline aquifers or depleted gas reservoirs, the complex interaction of CO_2 and impurities with reservoir fluids can lead to the formation of various solid phases, which can significantly affect the injectivity of wells and cause formation damage. The accumulation of solids in the pore space causes a reduction in porosity and, consequently, permeability. Notice that even a small reduction in porosity can dramatically reduce rock permeabilities.

Injected CO_2 will displace resident brine, while connate water will slowly evaporate into the CO_2-rich phase. Even though solubility of H_2O into supercritical CO_2 is very low, a continuous injection stream of dry CO_2 can lead to almost complete formation dry-out in the near-wellbore region (Ott et al., 2015). As a result, dissolved solids in the highly saline residual brine may start to precipitate. Furthermore, the Joule-Thomson cooling that is accompanied by the rapid expansion of injected CO_2 into the reservoir may be large (Oldenburg, 2007). With the presence of H_2O and hydrate-forming gases (e.g., CO_2 or, in depleted gas reservoirs, CH_4) accompanied by low temperatures and high pressures, this could be sufficient to trigger formation of hydrates, also resulting in porosity reduction. This mechanism could pose potential problems in depleted hydrocarbon reservoirs in particular, where Joule-Thomson cooling is more pronounced.

In this work, we present a unified simulation framework that can capture the potential near-wellbore effects induced by CO_2 injection. The framework is developed using the Delft Advanced Research Terra Simulator (DARTS) platform (Khait and Voskov, 2018b; Lyu et al., 2021). DARTS uses the Operator-Based Linearization (OBL) technique for incorporating all complex physical phenomena in a fully coupled fully implicit manner (Voskov, 2017; Khait and Voskov, 2018a). A general multicomponent multiphase flash based on a combination of classic cubic equations of state for hydrocarbon/CO_2-rich phases and an activity model for the aqueous phase is implemented following Ziabakhsh-Ganji and Kooi (2012); Ballard (2002). The activity model incorporates the effect of brine molality on phase behaviour, that translates into altered mutual solubilities of gases and water in the aqueous and the CO_2-rich phases, respectively. Moreover, kinetic mechanisms of salt precipitation and hydrate formation are treated in a unified manner. Equilibrium behaviour for ion and salt components is described by an activity product (Kala and Voskov, 2020), whereas hydrate phase behaviour is modelled using a modified Van der Waals-Platteeuw hydrate equation of state (Van der Waals and Platteeuw, 1959; Ballard, 2002). Accurate treatment of thermophysical properties - most notably, enthalpy - enables the DARTS framework to capture important thermodynamic phenomena, such as the Joule-Thomson effect and the endo-/exothermic nature of reactions and phase changes.

We demonstrate that all-important physical phenomena, including the Joule-Thomson effect, salt precipitation and hydrate formation can be effectively captured by the OBL approach. We use several existing numerical benchmarks to validate the accuracy of the developed framework in the dynamic representation of all these effects.

Theory and method

In this section, the unified thermal-reactive compositional simulation framework will be outlined. Then, thermodynamic calculations involving both phase equilibrium and a kinetic formulation of chemical reactions will be described. In addition, thermal properties can be derived from thermodynamic relations.

Residual formulation of conservation equations

In this work, fluid flow is governed by advective and diffusive fluxes. For mass components, the transport equation can be expressed as

$$\frac{\partial}{\partial t}\left(\phi \sum_{j=1}^{n_p} \rho_j s_j x_{cj}\right) = -\nabla \cdot \left(\sum_{j=1}^{n_p} x_{cj}\rho_j \boldsymbol{u}_j + s_j \rho_j \mathbf{J}_{cj}\right) + \sum_{j=1}^{n_p} x_{cj}\rho_{mj}q_j + \sum_{k=1}^{n_k} v_{ck}r_k \quad c = 1,...,n_c \quad (1)$$

The energy conservation equation accounts for advective and conductive heat flow and contains contributions from both pore fill and rock:

$$\frac{\partial}{\partial t}\left(\phi \sum_{j=1}^{n_p} \rho_j s_j U_j + (1-\phi)U_r\right) = -\nabla \cdot \left(\sum_{j=1}^{n_p} h_j\rho_j \boldsymbol{u}_j + \kappa\nabla T\right) + \sum_{j=1}^{n_p} h_j\rho_j\hat{q}_j \tag{2}$$

Here, the velocity $\boldsymbol{u}_j$ follows the extension of Darcy's law for multiphase flow, which includes gravitational and capillary effects:

$$\boldsymbol{u}_j = \mathbf{K}\frac{k_{rj}}{\mu_j}(\nabla p_j - \boldsymbol{\gamma_j}\nabla z), \tag{3}$$

The diffusive flux $\mathbf{J}_{cj}$ of component c in phase j is described by Fick's law as

$$\mathbf{J}_{cj} = -\phi\mathbf{D}_{cj}\nabla x_{cj}, \tag{4}$$

The rock is assumed compressible and the change of porosity is represented by

$$\phi = \phi_0\big(1 + c_r(p - p_{ref})\big) \tag{5}$$

The nonlinear equations are discretized using finite volume discretization with a two-point flux approximation and upstream weighting in space and a backward Euler approximation in time. The discretized residual form for a reservoir block i reads

$$R_i^c = V_i\Big(M_i^c(\omega_i) - M_i^c(\omega_i^n)\Big) - \Delta t\Big(\sum_l A_l F_l^c(\omega) + V_i Q_i^c(\omega)\Big) = 0, \quad c = 1,\dots,n_c+1. \tag{6}$$

Operator form of conservation equations

The Operator-Based Linearization (OBL) approach significantly simplifies the implementation of the complex simulation framework by introducing algebraic operators that capture all complex physics and nonlinear terms. Instead of keeping track of each property and its derivatives with respect to nonlinear unknowns, abstract algebraic operators representing the physics can be constructed and assembled into the set of Jacobian and residuals defined at each iteration. In the described approximation method, pressure, temperature and overall composition are taken as the unified state variables in a given control volume. Upstream weighting of the physical state is used to determine the flux-related fluid properties determined at the interface l. The discretized mass conservation equation in operator form for each grid block reads

$$V\phi_0[\alpha_c(\omega) - \alpha_c(\omega_n)] - \Delta t \sum_{l\in L(i)} \sum_{j=1}^{n_p} \big[\Gamma^l\beta_{cj}^l(\omega^u)\Delta\psi_j^l + \Gamma_d^l\gamma_j^l(\omega)\Delta\chi_{cj}\big] + \Delta tV\delta_c(\omega) = 0, \quad c = 1,\dots,n_c \tag{7}$$

Here we define the following state-dependent operators,

$$\alpha_{cf}(\omega) = \Big(1 + c_r(p - p_{ref})\Big)\sum_{j=1}^{n_p} x_{cj}\rho_j s_j, \ c = 1,\dots,n_c; \tag{8a}$$

$$\beta_{cj}(\omega) = x_{cj}\rho_j k_{rj}/\mu_j, \ c = 1,\dots,n_c, \ j = 1,\dots,n_p; \tag{8b}$$

$$\gamma_j(\omega) = \Big(1 + c_r(p - p_{ref})\Big)s_j, \ j = 1,\dots,n_p; \tag{8c}$$

$$\chi_{cj}(\omega) = D_{cj}\rho_j x_{cj}, \ c = 1,\dots,n_c, \ j = 1,\dots,n_p; \tag{8d}$$

$$\delta_c(\omega) = \sum_{j=1}^{n_p} v_{cj}r_j(\omega), \ c = 1,\dots,n_c. \tag{8e}$$

The phase-potential-upwinding (PPU) strategy for OBL parametrization is applied to model the gravity and capillary effect. The potential difference of phase j on the interface l between block 1 and 2 can be written as

$$\Delta\psi_j^l = p_1 - p_j^c(\omega_1) - (p_2 - p_j^c(\omega_2)) - \frac{\rho_j(\omega_1) + \rho_j(\omega_2)}{2}g(z_2 - z_1), \tag{9}$$

where p_j^c is the capillary pressure.

The discretized energy conservation equation can be written in operator form as:

$$V\phi_0[\alpha_{ef}(\omega) - \alpha_{ef}(\omega_n)] - \Delta t \sum_{l \in L(i)} \sum_{j=1}^{n_p} [\Gamma^l \beta_{ej}^l(\omega^u)\Delta\psi_j^l + \Gamma_d^l\gamma_j(\omega)\Delta\chi_{ej}] + \Delta t V \delta_e(\omega)$$

$$+ (1-\phi_0)VU_r[\alpha_{er}(\omega) - \alpha_{er}(\omega_n)] - \Delta t \sum_l (1-\phi_0)\Gamma_d^l\kappa_r\alpha_{er}(\omega)\Delta\chi_{er} = 0, \tag{10}$$

where

$$\alpha_{ef}(\omega) = \left(1 + c_r(p - p_{ref})\right)\sum_{j=1}^{n_p} \rho_j s_j U_j; \tag{11a}$$

$$\beta_{ej}(\omega) = h_j\rho_j k_{rj}/\mu_j, \ j = 1, \ldots, n_p; \tag{11b}$$

$$\chi_{ej}(\omega) = \kappa_j T_j, \ j = 1, \ldots, n_p; \tag{11c}$$

$$\delta_e(\omega) = \sum_{j=1}^{n_j} v_{ej} r_{ej}(\omega) \tag{11d}$$

In addition, three more operators to account for the energy of rock should be defined:

$$\alpha_{eri}(\omega) = \frac{U_r}{1 + c_r(p - p_{ref})}, \ \alpha_{erc}(\omega) = \frac{1}{1 + c_r(p - p_{ref})}, \ \chi_{er}(\omega) = T_r. \tag{12}$$

α_{eri} and α_{erc} represent the rock internal energy and rock conduction, respectively. U_r is a state dependent parameter, thus these two rock energy terms are treated separately. In this form, the nonlinear system is defined only in terms of physical state-dependent operators. The values of these operators are uniquely determined in the parameter space of the simulation problem with the set of primary unknowns. Approximation interpolants are generated at each point in the discrete parameter space at the pre-processing stage and stored in $(n_c + 1)$-dimensional tables.

Thermodynamic equilibrium

In this work, the CO_2-CH_4-brine system is modelled as a seven-component system with CO_2, CH_4, H_2O, Na^+, Cl^-, solid $NaCl$ and solid gas hydrate. The CO_2, CH_4 and H_2O components can occur in both the CO_2/CH_4-rich and the aqueous phase, the ions Na^+ and Cl^- are assumed to be present in the aqueous phase only and the solid components are in a separate solid phase. In describing the thermodynamic behaviour of the system, an exact local thermodynamic equilibrium between fluid phases is assumed. The solid phases are not taken into account in the phase equilibrium calculations but are modelled using the kinetic description.

At thermodynamic equilibrium, pressure and temperature are uniform throughout the system. Furthermore, a necessary condition for equilibrium is that the chemical potential for each component is the same throughout all phases, or, equivalently, that the fugacities of the individual components are equal:

$$\hat{f}_i^j(T, P, \boldsymbol{x}) = \hat{f}_i^k(T, P, \boldsymbol{y}), \quad i = 1, \ldots, n_c \tag{13}$$

between all phases j and k.

Following Michelsen and Mollerup (2007), a material balance for each component yields

$$x_{i0} + \sum_{j=1}^{n_p-1} v_j(x_{ij} - x_{i0}) = z_i, \quad i = 1, \ldots, n_c \tag{14}$$

with phase 0 the reference phase. Finally, mole fractions in the different phases must sum to unity, yielding

$$\sum_{i=1}^{n_c}(x_{ij}-x_{i0})=0, \quad j=1,\ldots,n_p-1. \tag{15}$$

For two phases, this sums to a total of $2n_c+1$ relations between the $2n_c+3$ unknowns, $\mathbf{x},\mathbf{y},T,P,\nu_1$. In $P-T$ flash, the phase equilibrium is defined by fixed pressure and temperature, resulting in $2n_c+1$ equations and $2n_c+1$ unknowns, $\mathbf{x},\mathbf{y},\nu_1$.

Convergence to a solution of equal fugacities (13) can be achieved with a successive substitution method. Introducing equilibrium factors $K_i=y_i/x_i$ in the material balance (14) yields

$$x_i=\frac{z_i}{1+\nu_1(K_i-1)}, \tag{16a}$$

and

$$y_i=\frac{z_iK_i}{1+\nu_1(K_i-1)}. \tag{16b}$$

Substituting these relations into the mole fraction relation (15) gives the Rachford-Rice equation for two phases:

$$\sum_{i=1}^{n_c}(y_i-x_i)=\sum_{i=1}^{n_c}\frac{z_i(K_i-1)}{1+\nu_1(K_i-1)}=0. \tag{17}$$

The equilibrium factors can be related to fugacity by substituting

$$\hat{f}_i^j=x_i\hat{\varphi}_i^jP, \quad \hat{f}_i^k=y_i\hat{\varphi}_i^kP, \tag{18}$$

where $\hat{\varphi}_i^j$ is the fugacity coefficient of component i in phase j. Then, the equilibrium factors can be written as

$$K_i=\frac{y_i}{x_i}=\frac{\hat{\varphi}_i^j}{\hat{\varphi}_i^k}. \tag{19}$$

To initiate the algorithm, a set of composition-independent equilibrium factors is used. During each iteration of successive substitution, component fugacities are held fixed, and the Rachford-Rice equation (17) is solved. Then, phase compositions can be determined from (16), which are used for re-evaluation of the fugacity coefficients. This process is repeated until (13) is honoured. In this study, classical cubic equations of state (Soave, 1972; Peng and Robinson, 1976) are used to evaluate the behaviour of the CO_2-rich phase and an activity model (Ballard, 2002; Ziabakhsh-Ganji and Kooi, 2012) is used for the aqueous phase. In each iteration, ion molality in the aqueous phase is re-calculated and used in the evaluation of fugacities.

Kinetic reactions

In a simple CO_2-CH_4-brine system, two types of reactions may occur. Ions dissolved in the brine may precipitate to form solid salt components when maximum solubility is exceeded. Furthermore, the presence of H_2O and hydrate-forming gases (CO_2 or CH_4) accompanied by low temperatures and high pressures could be sufficient for forming hydrates.

In chemically reacting systems, the assumption of instantaneous equilibrium is not always reasonable and a kinetic reaction mechanism might be required. As the system is away from equilibrium, it continuously attempts to reach chemical equilibrium through the formation and dissociation of phases, driven by the difference in chemical potential. At thermodynamic and chemical equilibrium, the system has reached its condition of maximum thermodynamic stability and there is no potential to alter the mass distribution among the phases.

Precipitation of NaCl is described as

$$\text{Na}^+{}_{(aq)} + \text{Cl}^-{}_{(aq)} \rightleftharpoons \text{NaCl}_{(s)}. \tag{20}$$

For this reaction, equilibrium behaviour is modelled using the activity product, given as

$$Q = \frac{[\text{NaCl}]}{[\text{Na}^+][\text{Cl}^-]}. \tag{21}$$

At equilibrium, Q is equal to the equilibrium product: $Q = K^{eq}$. In this work, ion activities are approximated by mole fraction as a simplification. The activity of the solid is assumed to be unity.

The rate at which the reaction takes place is generally expressed as:

$$r_k = c_k A_s \left(1 - Q/K^{eq}\right), \tag{22}$$

where c_k is a reaction constant and A_s is the reacting surface area.

For single component sI-type hydrate formation, which is not an actual chemical reaction, but merely a phase change that is better described by a kinetic mechanism, a pseudo-reaction reads

$$\text{G} + \text{n}_\text{H}\,\text{H}_2\text{O} \rightleftharpoons \text{G} \cdot \text{n}_\text{H}\text{H}_2\text{O}, \tag{23}$$

where G is a hydrate-forming gas component (e.g., CH_4 or CO_2) and n_H denotes the hydration number, corresponding to the number of water molecules bound to each guest molecule. Hydrates are non-stoichiometric substances, that is, it has no set chemical composition. Full cage occupancy of sI-hydrate would correspond to 8 gas molecules per 46 H_2O molecules and yields a hydration number of 5.75. However, it is thermodynamically more stable to fill only part of the cavities. Generally, the hydration number is approximately 6, depending on the thermodynamic state of the system. In this work, we assume a constant hydration number $n_H = 6.1$, which is in the range of reported values (Ballard, 2002).

For hydrates, equilibrium behaviour is described by the difference in fugacity of water between hydrate and non-hydrate phases. If hydrate fugacity is higher, hydrates will dissociate. If the fugacity of water in the non-hydrate phases is higher, hydrates will form. Following the formulation used by Kowalsky and Moridis (2007), the kinetic rate of hydrate formation or dissociation is given by

$$r_k = c_k A_s \exp\left(\frac{-\Delta E}{RT}\right)\left(f_{w,H} - f_{w,j}\right). \tag{24}$$

A difference in the fugacity of water between hydrate and non-hydrate phases is considered the driving force of the reaction. Assuming equal fugacity of hydrate guests in hydrate and non-hydrate phases, the fugacity of water in the hydrate phase is calculated using a modified Van der Waals-Platteeuw model (Van der Waals and Platteeuw, 1959), as described by Ballard (2002). For the other reaction parameters, where c_k is a reaction constant, A_s is the hydrate surface area and temperature is accounted for using an Arrhenius-type exponential factor that takes into account the activation energy of the reaction, we use the values reported by Kowalsky and Moridis (2007).

Treatment of solids

With solid phases present in the pores, pore space occupied by fluid phases is reduced and, consequently, the ability for flow is decreased. To account for this effect, a porosity-permeability relationship is implemented. Dividing the pore volume into fractions occupied by fluid phases f, reactive solid r and non-reactive solid nr gives

$$1 = \phi_f + \phi_r + \phi_{nr}. \tag{25}$$

The total volume fraction available for the mass components in the conservation equations $\phi^T = \phi_f + \phi_r$ remains constant over the course of simulation (that is, when neglecting compressibility) and is equal to the sum of the fluid and reactive solid fractions.

Table 1: Input for determination of kinetic rates

Parameter	$Na^+ + Cl^- \rightleftharpoons NaCl$	$CH_4 + n_H H_2O \rightleftharpoons CH_4 \cdot n_H H_2O$
Fugacity or activity	$x_{i,Aq}$ for ions, 1 for NaCl	Peng and Robinson (1976), Soave (1972), Ziabakhsh-Ganji and Kooi (2012), Ballard (2002)
Surface area A_s	1 m^2/m^3	Yin et al. (2018)
Activation energy ΔE	n.a.	81 kJ/mol
Reaction constant c_k	0.1 kmol/m^2.day	$3.11 \cdot 10^{12}$ kmol/m^2.bar.day
Equilibrium constant K^{eq}	100	n.a.

In order to account for the permeability reduction, a permeability multiplier is calculated from the fluid volume fraction. The fraction of pore space available for fluid phases is calculated from

$$\phi_f = \phi^T \left(1 - \sum_{s=1}^{n_s} s_s\right). \tag{26}$$

Then, the permeability reduction is applied through

$$T^r = T \cdot \left(\frac{\phi_f}{\phi^T}\right)^n, \tag{27}$$

where T^r is the reduced transmissibility, T is initial transmissibility and n is an exponent.

Enthalpy from residual thermodynamics

Enthalpy of a system can be defined as the sum of mixture ideal gas enthalpy and residual enthalpy, which is the difference between the enthalpy of a real mixture and that of an ideal gas. From thermodynamic models, residual enthalpies can be calculated from the derivative of the fugacity coefficient with respect to temperature according to

$$H_i^r(T, P, \mathbf{n}) = -RT^2 \left(\frac{\partial \ln \hat{\varphi}_i}{\partial T}\right)_{P,\mathbf{n}}, \tag{28a}$$

or

$$H_i^r(T, P, \mathbf{n}) = -RT^2 \left(\frac{\partial \ln \hat{f}_i}{\partial T}\right)_{P,\mathbf{n}}, \tag{28b}$$

which then add up to total mixture residual enthalpy as

$$H^r(T, P, \mathbf{n}) = \sum_i n_i H_i^r(T, P, \mathbf{n}). \tag{29}$$

Then, the enthalpy of the mixture in the ideal gas state is a summation of individual ideal gas enthalpies:

$$H^*(T, \mathbf{n}) = \sum_i n_i H_i^*(T), \tag{30}$$

with $H_i^*(T)$ the pure component enthalpy relative to a reference temperature T_0.

Note that, in our formulation (2), enthalpy changes related to reactions, phase changes and the Joule-Thomson effect are included implicitly through the consistent treatment of enthalpy. The temperature change accompanied by a pressure change is defined by the Joule-Thomson coefficient

$$\frac{\Delta T}{\Delta P} \approx \left(\frac{\partial T}{\partial P}\right)_H = \mu_{JT}. \tag{31}$$

For most common gases at conditions of interest, μ_{JT} is positive, and consequently the temperature drops with a pressure drop. However, below the Joule-Thomson inversion temperature, the expansion will result in a temperature increase and the sign of μ_{JT} is negative.

Numerical results

In this section, we present various benchmarks validating our simulation framework.

Joule-Thomson effect

We have tested the ability of the OBL technique to represent the Joule-Thomson effect using a simple setup proposed by Oldenburg (2007). A one-dimensional four-gridblock mesh, consisting of a large volume on both sides of a low-permeability block and a monitoring block, is constructed. Pressure and temperature in the left block remain constant. Pressure in the right block is also constant, such that gas flows from left to right. The pressure drop occurs almost entirely over the low permeability block. The temperature change is recorded in the monitoring block and the Joule-Thomson coefficient is calculated from (31).

The experiment has been carried out over a range of pressure and temperature to determine the Joule-Thomson coefficient for CO_2. In Figure 1, the results for Peng and Robinson (1976) and Soave (1972) equations of state in our framework have been compared to values reported in NIST Chemistry Web-Book.
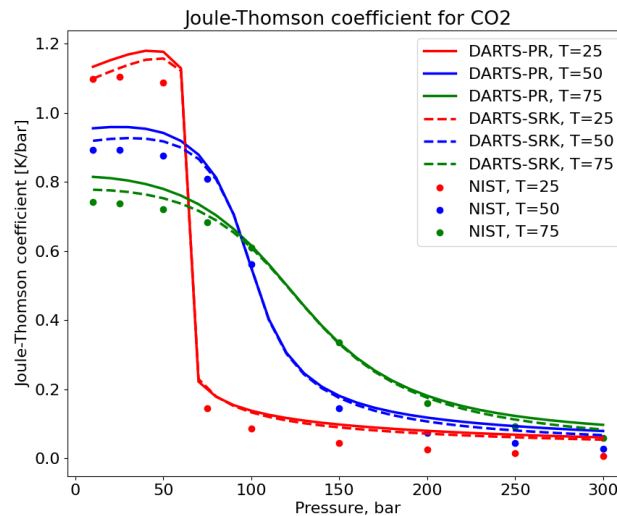

Figure 1: Results of Joule-Thomson experiment for different EOS compared to NIST Chemistry Web-Book

The obtained results are within the accuracy of results reported in Oldenburg (2007). Based on these observations, it is clear that the OBL approach is capable of capturing the Joule-Thompson effect and reproduce the realistic behavior of CO_2-gas-brine systems.

Salt precipitation

Drying out of saline formations upon dry gas injection, accompanied by precipitation of salt dissolved in brines, is another important phenomenon in CO_2 sequestration applications. Ott et al. (2015) have addressed this issue in a series of experimental and numerical studies. Following the experiments described by Ott et al. (2015), we illustrate the mechanism of salt precipitation from residual brine, which is vaporized by the dry supercritical CO_2 injection stream. The input used for calculating kinetic rates of this reaction has been summarized in Table 1. Note that, in this simulation, the input parameters for kinetic rates are not meant to represent the reaction kinetics accurately, but merely to demonstrate the salt precipitation mechanism in the process of drying out of formations. All parameters in simulation follow the experimental setup from Ott et al. (2015).

We emphasize the importance of accurate treatment of salinity in the activity model for the aqueous phase, as this affects the solubility of H_2O in the CO_2-rich phase. This ultimately controls evaporation and thus the propagation of the trailing shock. We compare the simulation results shown in Figure 2 with a simulation where we neglect the presence of ions in the calculation of fugacities. The difference can be observed in Figure 2 where the vaporizing front is propagating slower in the case where brine molality is accounted for in the phase behaviour, which results from the lower solubility of H_2O in the CO_2 injection stream.
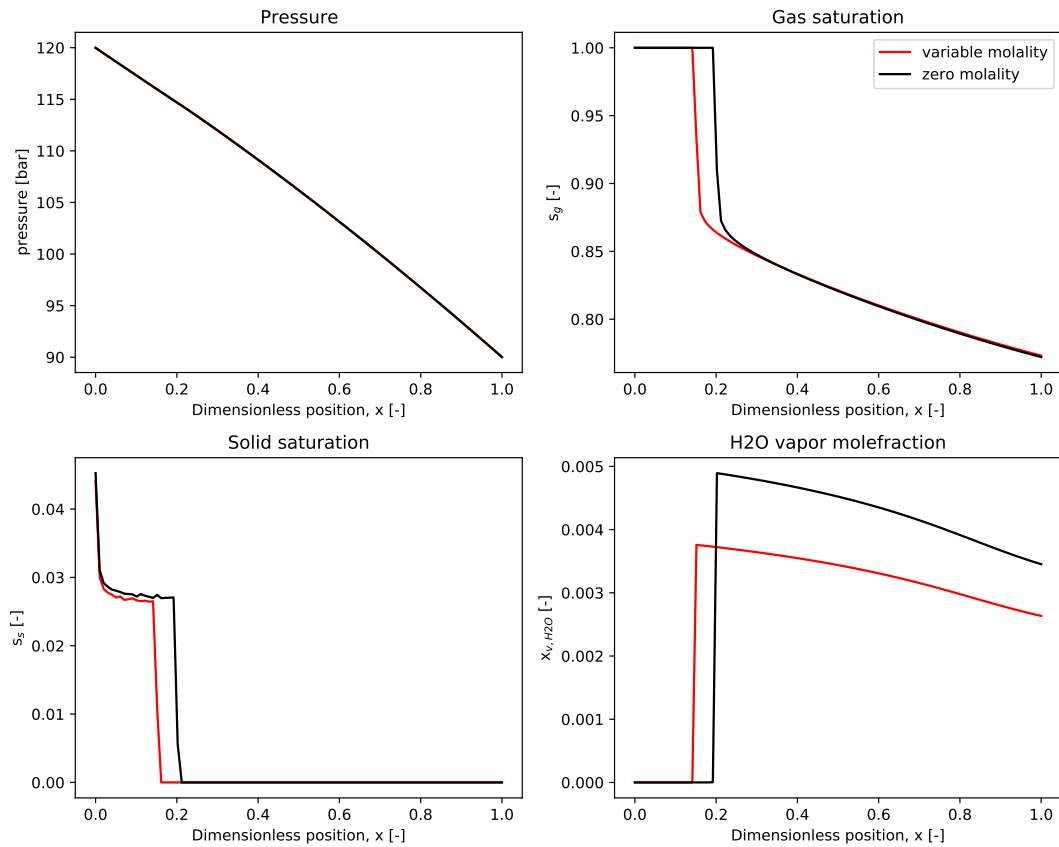

Figure 2: Simulation results of conceptual formation dry-out model in DARTS

To conclude the salt precipitation results, in Figure 3 we present simulation in 2D core analogue model. These results are in qualitative agreement with our ongoing experimental study and we are currently in the process of quantitative validation of these simulations with inclusion of capillary pressure.

Hydrate formation and dissociation

Finally, we demonstrate the ability of our simulation framework to capture the processes of formation and dissociation of hydrates. Studies on hydrate-bearing geological formations are often focused on sI-type methane hydrates, which represent the most occurring type of hydrates in nature. Although the formation of CO_2-hydrates triggered by gas injection involves different guest molecules, thermodynamic calculations for pure CH_4- or CO_2-hydrates are similar, as long as no binary CH_4-CO_2 hydrates are considered. The simulation studies in this section concern single-guest hydrates. The input used for the determination of kinetic rates of hydrate formation and dissociation has been summarized in Table 1.

The formation of methane hydrates in porous media has been studied by Yin et al. (2018). They performed a numerical analysis of experiments in which the hydrate formation process in a small reactor was observed. Here, we attempted to carry out the same numerical simulation during the first formation stage (denoted F1), as shown in Figure 4. The core is brought into hydrate formation conditions by lowering the temperature. As hydrates form, methane and water are consumed to form the hydrate phase,
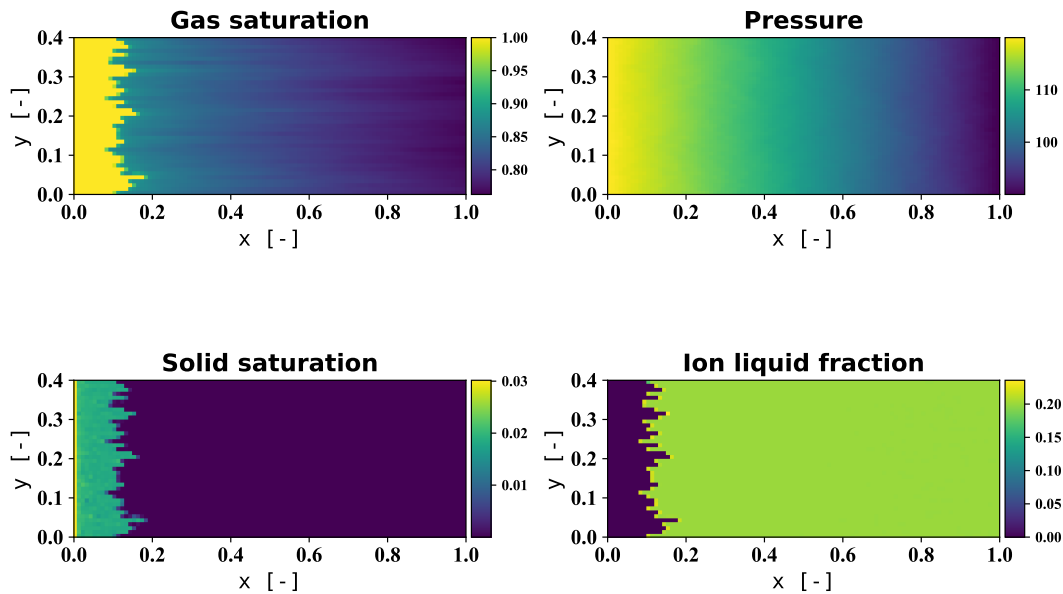
Figure 3: Salt precipitation in 2D core analogue

resulting in a decrease in pressure. In the graphs, changes in (a) pressure, (b) temperature and (c) mass of components are displayed over time. We must note that in our simulation framework, modelling of the temperature boundary conditions is restricted and to perform the simulation, the model was re-initialized regularly with temperatures following the experimental values reported by Yin et al. (2018). This causes a slight deviation between the two results.

The dissociation behaviour of methane hydrates in relation to gas production has been studied by Kowalsky and Moridis (2007). They compared the use of kinetic and equilibrium reaction models in the simulation of various hydrate production methods, such as depressurization and thermal stimulation. In this study, we perform a simulation of the depressurization-induced production case, as displayed in Figure 5. Here, we compare a simulation in the segment reservoir meshed with an unstructured grid which explains more dispersive results in comparison to Kowalsky and Moridis (2007) where a radial grid has been used.

It can be observed that a pressure shock travels through the reservoir, along which hydrates dissociate. Temperature declines with hydrate dissociation, due to the endothermic nature of this process. Furthermore, cooling is enhanced by expanding gas released from dissociating hydrates. We can consider based on these experiments that simulation with the OBL approach captures the complex phenomena associated with hydrate formation with acceptable accuracy.

Conclusions

In this study, we have formulated a unified simulation framework that is capable of capturing important physical phenomena relevant to near-wellbore effects induced by CO_2 injection into saline aquifers or depleted hydrocarbon reservoirs. The OBL technique offers flexibility for incorporating complex physics and proves to be effective to include a range of physical processes. In this work, we have combined accurate thermodynamic modelling of fluid phases, including treatment of brine molality, kinetic formulations for salt precipitation and hydrate formation reactions and consistent implementation of thermophysical properties to demonstrate the applicability of the OBL technique to a simulation of
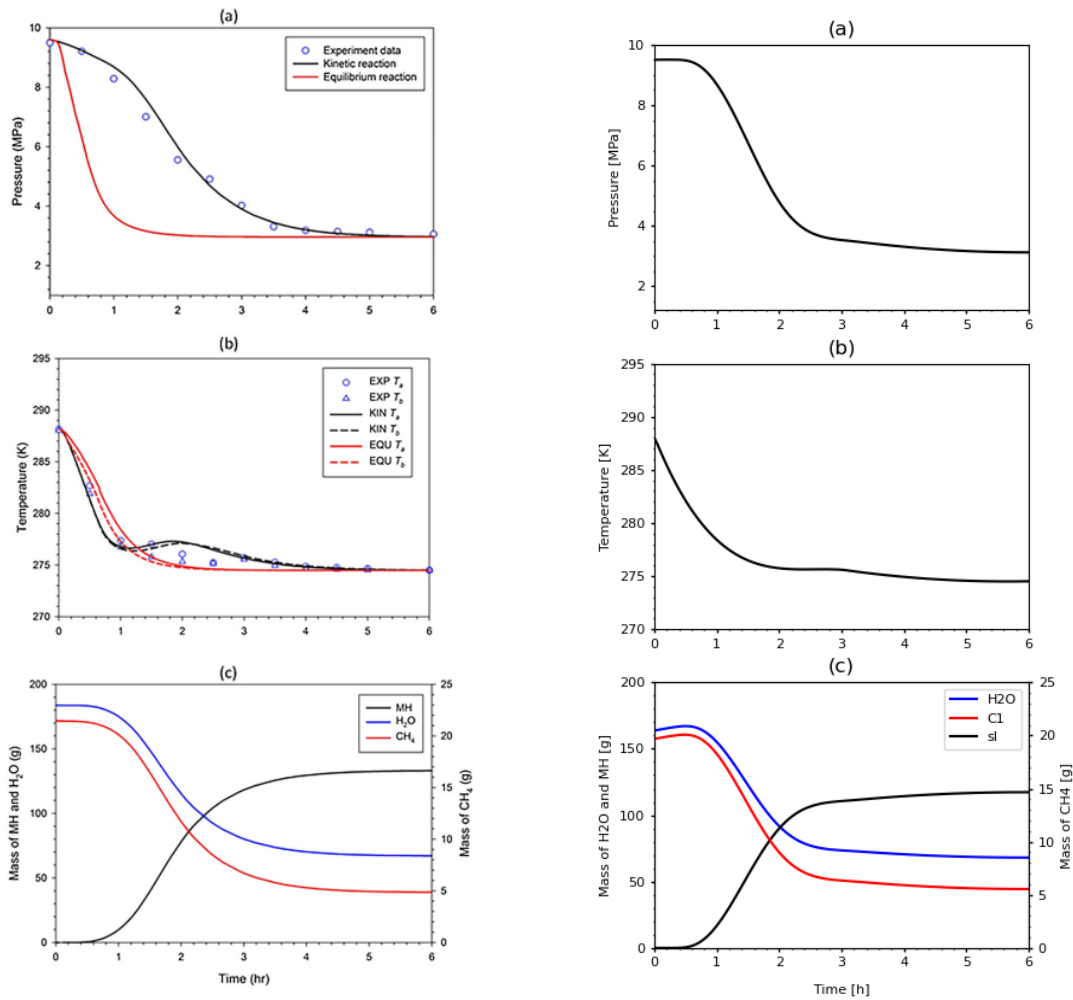
Figure 4: Simulation results of F1 methane hydrate formation stage in DARTS (right) compared to Yin et al. (2018) (left) with evolution over time of (a) pressure, (b) temperature and (c) total mass of components.

CO_2-related problems. The framework has been tested and compared with existing numerical benchmarks that address the Joule-Thomson effect, salt precipitation associated with dry-out of porous rock and formation and dissociation of gas hydrates. We demonstrate that the DARTS framework is capable of reproducing the complex behaviour of CO_2-brine systems observed in other work with reasonable accuracy.

Future work will extend the current capabilities to include the mechanism of capillary backflow in modelling the dry-out effect, which could allow accumulation of significant amounts of solid salt. Another ongoing effort is to accurately represent brine chemistry using fully-implicit coupling with external chemical equilibrium software (Reactoro) combined with accurate kinetics and taking into account rock heterogeneity. We will validate the accuracy of our models with on-going experimental work. Furthermore, accurate modelling of hydrate behaviour will involve systems with brines and a mixture of gases. The validity of the simulation framework for modelling near-wellbore effects can then be tested for complex reservoir scenarios.
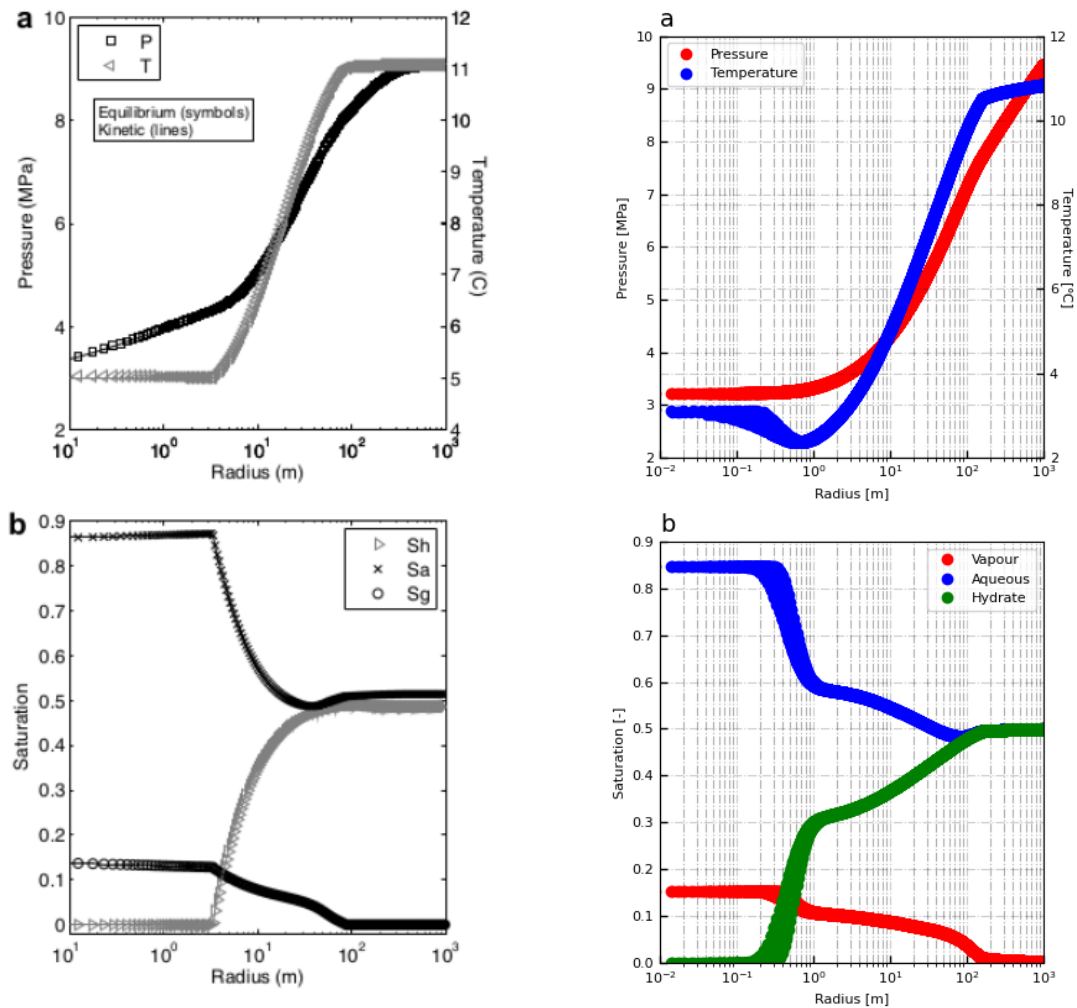
Figure 5: Simulation results of methane hydrate dissociation experiment in DARTS (right) as performed by Kowalsky and Moridis (2007) (left) with (a) pressure and temperature and (b) phase saturations after 30 days. The x-axis is logarithmic in scale.

Acknowledgements

References

Ballard, A.L. [2002] *A non-ideal hydrate solid solution model for a multi-phase equilibria program.* Ph.D. thesis, Colorado School of Mines.

Kala, K. and Voskov, D.V. [2020] Element balance formulation in reactive compositional flow and transport with parameterization technique. *Computational Geosciences*, **24**, 609–624.

Khait, M. and Voskov, D.V. [2018a] Adaptive parameterization for solving of thermal/compositional nonlinear flow and transport with buoyancy. *SPE Journal*, **23**(02), 522–534.

Khait, M. and Voskov, D.V. [2018b] Operator-based linearization for efficient modeling of geothermal

processes. *Geothermics*, **74**, 7–18.

Kowalsky, M.B. and Moridis, G.J. [2007] Comparison of kinetic and equilibrium reaction models in simulating gas hydrate behavior in porous media. *Energy conversion and management*, **48**(6), 1850–1863.

Lyu, X., Khait, M. and Voskov, D.V. [2021] Operator-Based Linearization Approach for Modelling of Multiphase Flow with Buoyancy and Capillarity. *SPE Journal*, 1–18.

Michelsen, M.L. and Mollerup, J.M. [2007] *Thermodynamic Models: Fundamentals & Computational Aspects*. Tie-Line Publications.

Oldenburg, C.M. [2007] Joule-Thomson cooling due to CO_2 injection into natural gas reservoirs. *Energy Conversion and Management*, **48**, 1808–1815.

Ott, H., Roels, S. and de Kloe, K. [2015] Salt precipitation due to supercritical gas injection: I. Capillary-driven flow in unimodal sandstone. *International Journal of Greenhouse Gas Control*, **43**, 247–255.

Peng, D.Y. and Robinson, D.B. [1976] A new two-constant equation of state. *Ind. Eng. Chem., Fundam.*, **15**(1), 59–64.

Soave, G. [1972] Equilibrium constants from a modified Redlich-Kwong equation of state. *Chemical Engineering Science*, **27**, 1197–1203.

Voskov, D.V. [2017] Operator-based linearization approach for modeling of multiphase multi-component flow in porous media. *Journal of Computational Physics*, **337**, 275–288.

Van der Waals, J. and Platteeuw, J. [1959] Clathrate solutions. *Advances in Chemical Physics*, **2**.

Whitson, C.H. and Michelsen, M.L. [1989] The negative flash. *Fluid Phase Equilibria*, **53**, 51–71.

Yin, Z., Moridis, G., Kiang Tan, H. and Linga, P. [2018] Numerical analysis of experimental studies of methane hydrate formation in a sandy porous medium. *Applied Energy*, **220**, 681–704.

Ziabakhsh-Ganji, Z. and Kooi, H. [2012] An Equation of State for thermodynamic equilibrium of gas mixtures and brines to allow simulation of the effects of impurities in subsurface CO_2 storage. *International Journal of Greenhouse Gas Control*, **11S**, S21–S34.